

Measured and modeled properties of mammalian skeletal muscle. II. The effects of stimulus frequency on force-length and force-velocity relationships

IAN E. BROWN¹, ERNEST J. CHENG² and GERALD E. LOEB^{2,*}

¹Division of Biology 216-76, California Institute of Technology, Pasadena, CA, 91125, USA; ²The MRC Group in Sensory-Motor Neuroscience, Department of Physiology, Queen's University, Kingston, ON, Canada, K7L 3N6

Received 10 August 1998; accepted in revised form 1 December 1998

Abstract

Interactions between physiological stimulus frequencies, fascicle lengths and velocities were analyzed in feline caudofemoralis (CF), a hindlimb skeletal muscle composed exclusively of fast-twitch fibers. Split ventral roots were stimulated asynchronously to produce smooth contractions at sub-tetanic stimulus frequencies. As described previously, the peak of the sub-tetanic force-length relationship was found to shift to longer lengths with decreases in stimulus frequency, indicating a length dependence for activation that is independent of filament overlap. The sub-tetanic force-velocity (FV) relationship was affected strongly both by stimulus frequency and by length; decreases in either decreased the slope of the FV relationship around isometric. The shapes of the force transients following stretch or shortening revealed that these effects were not due to a change in the instantaneous FV relationship; the relative shape of the force transients following stretch or shortening was independent of stimulus frequency and hardly affected by length. The effects of stimulus frequency and length on the sub-tetanic FV relationship instead appear to be caused by a time delay in the length-dependent changes of activation. In contrast to feline soleus muscle, which is composed exclusively of slow-twitch fibers, CF did not yield at sub-tetanic stimulus frequencies for the range of stretch velocities tested (up to 2 L_0/s). The data presented here were used to build a model of muscle that accounted well for all of the effects described. We extended our model to account for slow-twitch muscle by comparing our fast-twitch model with previously published data and then changing the necessary parameters to fit the data. Our slow-twitch model accounts well for all previous findings including that of yielding.

Introduction

Mathematical models of muscle help us to understand and develop strategies for motor control, both for basic research (Gribble and Ostry, 1996; Krylow and Rymer, 1997; Loeb *et al.*, 1999) and for clinical restoration of movement to paralyzed limbs through functional electrical stimulation (see Chizeck, 1992). Both of these research directions require a muscle model that meets at least three criteria: (1) it should be sufficiently generic to be adaptable for many different systems and circumstances; (2) it should be as simple as possible; (3) it should predict accurately the force output of muscle under *physiological* operating conditions. Most current muscle models that attempt to meet these criteria (e.g. Otten, 1987; Durfee and Palmer, 1994; Brown *et al.*, 1996b) fall short of these goals because they assume that muscle properties scale with activation despite significant evidence to the contrary (although see Hatze, 1977). Over the physiologically relevant sub-tetanic stimulus frequencies (Bigland and Lippold, 1954;

Bellemare *et al.*, 1983; Hoffer *et al.*, 1987), important intrinsic properties of muscle, including the force-length (FL) and force-velocity (FV) relationships, have been shown to change (Joyce *et al.*, 1969; Rack and Westbury, 1969; Stephenson and Wendt, 1984; Roszek *et al.*, 1994; Balnave and Allen, 1996). Because the effects observed by these various researchers are substantial, the next generation of muscle models should be designed to account for these effects.

To create a 'next generation' muscle model we need physiologically relevant data sets upon which to base the model. We believe that such data sets should be collected from whole-muscle preparations rather than single-motor-unit or single-fiber preparations primarily because both single-motor-unit and single-fiber preparations cannot produce smooth contractions at physiological sub-tetanic stimulus frequencies. In contrast, asynchronous stimulation of separate bundles of motor axons for a whole muscle can simulate the smooth contractions that occur normally when motor units are recruited physiologically (as introduced by Rack and Westbury, 1969). One side-effect of this choice is that we must use muscles composed exclusively of one fiber type for our experiments so as to be able to measure the effects of slow-twitch and fast-twitch muscle fibers independently.

*To whom correspondence should be addressed: Department of Biomedical Engineering, University of Southern California, Los Angeles, CA 90089. Fax: 213 821-1120. E-mail: GLoeb@BMSR.usc.edu

Early this century (e.g. Cooper and Eccles, 1930), feline soleus (SOL), an ankle extensor, was identified as a useful whole-muscle preparation because of its high slow-twitch fiber content (estimated at 100% by Ariano *et al.*, 1973). Since then a few studies have examined the contractile characteristics of SOL at sub-tetanic stimulus frequencies (e.g. Joyce *et al.*, 1969; Rack and Westbury, 1969; Nichols and Houk, 1976). However, little comparative work has been conducted on an appropriate fast-twitch counterpart to SOL. Recently, Brown *et al.* (1998b) identified feline caudofemoralis (CF), a hip extensor/adductor, as a particularly suitable preparation in which to conduct such experiments. CF was found to have a simple, parallel-fibered architecture with no pennation angle and an almost exclusively fast-twitch fiber composition (95–100%). CF also has a high ratio of fascicle length to aponeurosis length (ca. 5:1), which results in a whole-muscle preparation with very little in-series compliance.

The main objective of this study was to collect physiologically relevant data on the effects of steady-state sub-tetanic stimulus frequencies on the FL and FV properties of potentiated fast-twitch muscle. The potentiated state was chosen as the base state for our model following a previous study in which we concluded that the normal operating state of fast-twitch muscle during repetitive tasks is, in fact, the potentiated state (Brown and Loeb, 1998b). We based this conclusion on the following observations: after a few sub-tetanic trains, a stable and near maximal level of potentiation can be reached; this stable level of potentiation can be maintained with low-intensity, intermittent activation; this stable level of potentiation disappears only after a long period of inactivity. Throughout this paper the phrase 'potentiated state' refers to this stable near-maximal level of potentiation. The effects of dynamic changes in stimulus frequency (e.g. rise and fall times) have been left for a subsequent paper in preparation as have the effects of stretch-induced force enhancement and shortening-induced force depression. A second objective of this study was to create a next-generation muscle model using this new data set together with previously published data collected from a slow-twitch muscle, feline SOL.

Our general approach to modeling is to design functions whose terms, where possible, have a one-to-one correspondence with anatomical structures and physiological processes within muscle. These functions are then characterized one at a time and their effects removed from the data to allow subsequent functions to be isolated and characterized. This approach makes it more straightforward to identify the key morphometric and functional characterization data required to adapt these models to different muscles. It also facilitates the use of these data and models to illuminate current issues in muscle physiology (Brown and Loeb, 1999a). A preliminary account of these findings has been published (Brown and Loeb, 1998a).

Materials and methods

Experimental data collection

The experimental apparatus and procedures used in this study are similar to those described previously for feline CF muscle (Brown and Loeb, 1998b). Experiments were carried out in 14 cats of either sex (2.6–5.4 kg) under deep pentobarbital anesthesia as determined by the absence of pedal withdrawal. Briefly, the feline CF muscle was dissected free of surrounding tissue with its origin, innervation and blood supply left intact. It was maintained thermostatically at $37 \pm 1^\circ\text{C}$ in a mineral oil pool. The length of the muscle fascicles was controlled by clamping onto caudal vertebrae Ca2 and Ca3 (CF origin) and onto the insertion tendon just at the point where the distalmost muscle fibers terminate. This eliminated virtually all series compliance in the linkage. The insertion clamp was attached to a computer-controlled muscle puller via a force transducer. Electrical stimulation was applied via platinum-iridium hook electrodes on cut L7 and S1 ventral roots and monitored by recording M-waves via two multi-stranded stainless steel wire electrodes inserted transversely through the muscle ca. 5 mm apart. Computer templates controlled the length, velocity and stimulus patterns simultaneously for long preprogrammed sequences defining entire experimental protocols in 1.667 ms steps. During each step, the computer program recorded values for both the force and a rectified, bin-integrated representation of the M-waves. Force was digitally filtered after the experiment using a double-pass, second-order Butterworth filter with a 3 dB cutoff frequency of 120 Hz to remove high-frequency (150–200 Hz) resonant noise from our system.

To produce smooth contractions at sub-tetanic stimulus frequencies, the ventral roots were split into five bundles that were stimulated asynchronously, analogous to the experiments performed on feline SOL by Rack and Westbury (1969). The maximal dispotentiated twitch force produced by each individual bundle ranged from 15–25% of the maximal dispotentiated twitch force produced by the whole muscle. In this study, stimulus frequency always refers to the frequency applied to each of the nerve bundles.

Near the beginning of each experiment a tetanic force-length (FL) curve was collected in the dispotentiated state. The dispotentiated state was maintained by inserting 5 min passive intervals between each stimulus train (Brown and Loeb, 1998b). Tetanic contractions (120 pps, 15 p trains) were elicited at the lengths estimated to correspond to 0.7, 0.8, 0.9, 0.95, 1.0, 1.05, 1.1 and 1.2 L_0 based upon *in situ* anatomical lengths (Brown *et al.*, 1998b; L_0 is the fascicle length at which maximal tetanic isometric force can be elicited). The 'true' L_0 was then chosen as the length at which maximal tetanic isometric force could be elicited. Sarcomere length measurements collected during these experiments demonstrated that the peak of the tetanic FL relation-

ship occurs reliably at ca. 2.4–2.5 μm , as expected based upon sliding filament theory. These data have been published previously as part of a larger study on CF morphometry (Brown *et al.*, 1998b).

All other stimulus paradigms in this series of experiments were conducted while CF was potentiated. These paradigms used stimulus trains that were always separated by 7 s. Potentiation was achieved by applying twelve isometric 10 p trains at 60 pps at three successive lengths (0.75, 0.95 and 1.15 L_0) and maintained with 15–120 pps stimulus trains (8–12 p duration). This protocol has been shown previously to provide a stable and apparently near-maximal level of potentiation in CF (Brown and Loeb, 1998b). Unless otherwise stated only one set of potentiated data of up to 45 stimulus trains was collected from each experiment to avoid the effects of low-frequency fatigue (Westerblad and Allen, 1991; Westerblad *et al.*, 1993) which can be quite strong in CF (Brown and Loeb, unpublished observations). For those experiments in which two potentiated data-sets were collected, the muscle and nerve preparations were allowed to relax for at least 45–60 min between each data set. In all paradigms stimulation voltage (0.2 ms rectangular pulses) was five times higher than the threshold required to elicit an M-wave. M-wave amplitude was monitored continuously to ensure complete recruitment of the entire muscle throughout the experiment. We applied single isometric twitches at 1.0 L_0 one second before specified stimulus trains so that peak twitch force could be used to monitor potentiation (Brown and Loeb, 1998b).

The model

The basic form of the muscle model proposed is similar to one suggested previously by Zajac (1989) and later refined by Brown *et al.* (1996b). A detailed explanation of our strategy can be found in Brown and Loeb (1999a). The model contains anatomically distinct elements shown schematically in Figure 1A. A series-elastic element (SE) represents the connective tissue at the muscle ends whereas an active contractile element (CE) in parallel with a passive elastic element (PE) represents the muscle fascicles. The SE was not investigated in this study because it was negligible for the operating conditions in our preparation (see Scott and Loeb (1995) and Brown *et al.* (1996b) for a complete description of SE properties). As discussed by Zajac (1989), for a model to be adaptable to muscles with different architectures, the inputs and outputs of the model elements need to be normalized. All forces are therefore normalized to units of F_0 (maximal potentiated isometric force). All series-elastic lengths are normalized by L_0^T (length of SE when stretched by F_0). All fascicle lengths and velocities are scaled by L_0 (fascicle length at which F_0 is elicited). Note that the length at which peak twitch force is elicited is usually 10–30% greater than L_0 and should not be used in its place (Close, 1972; Roszek *et al.*, 1994; Brown and Loeb, 1998b).

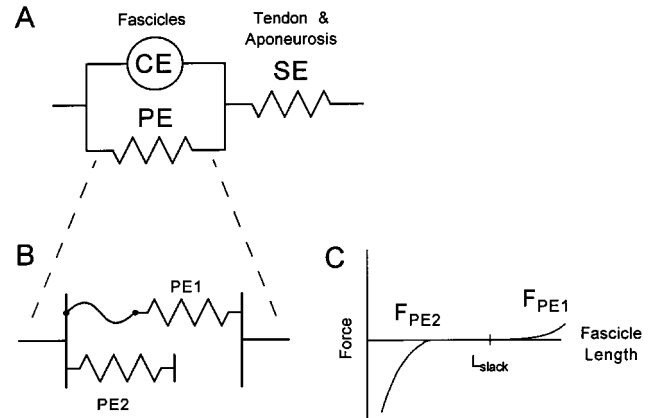


Fig. 1. A. Schematic of muscle model elements (based on model from Zajac, 1989 and Brown *et al.*, 1996b). The contractile element (CE) operates in parallel with the passive elastic element (PE) to represent the fascicles. The series-elastic element (SE) represents the combined tendon and aponeurosis. B, C. Passive elastic element. PE1 is the well recognized non-linear spring that resists stretch in the passive muscle, while PE2 is a non-linear spring resisting compression during active contraction at short lengths.

A mathematical summary of our model is provided in equations 1–3.

$$F = F_{CE} + F_{PE} \quad (1)$$

$$F_{CE} = R \cdot Af \cdot FL \cdot FV \quad (2)$$

$$F_{PE} = F_{PE1} + R \cdot Af \cdot F_{PE2} \quad (3)$$

A schematic description of these main elements and their associated sub-elements as developed in this study is provided in Figure 11. In equation 1, F is the total force produced by the muscle fascicles while F_{CE} and F_{PE} represent the forces produced by the CE and PE respectively; all three forces have units of F_0 . In equation 2, R is defined as the recruitment factor which represents the active or recruited fraction of muscle cross-sectional area and is a unitless quantity ($0 \leq R \leq 1$). For the data collected in this study recruitment was always equal to 1. Af is defined as the activation-frequency relationship and is also unitless ($0 \leq Af \leq 1$, $Af = 1$ for tetanic stimulation); Af depends primarily upon stimulus frequency and provides a measure of the fraction of available cross-bridges that are cycling in all recruited muscle fibers. FL is defined as the tetanic force-length relationship and has units of F_0 ($0 \leq FL \leq 1$); FL is primarily dependent upon fascicle length. FV is defined as the tetanic force-velocity relationship and is unitless ($FV = 1$ for isometric condition); FV depends primarily upon fascicle velocity which is defined as positive for lengthening velocities. The PE, as shown in Figure 1B and modeled in equation 3, has two spring-like components as originally proposed by Brown *et al.* (1996b). They have units of F_0 and are non-linear functions of length. When the slack is pulled out of the ideal, bendable, fixed-length linkage that connects spring PE1, it exerts a tensile force. At shorter fascicle lengths, the compression spring PE2 comes into play with a separate

spring function that resists compression (Figure 1C). As discussed by Brown *et al.* (1996b), PE2 represents the effects of compressing the thick filament at sarcomere lengths that are shorter than the thick filament; its contribution to F_{PE} scales with recruitment and activation as shown in equation 3 and as discussed in the Appendix.

The main purpose of this study was to collect a data set that could be used to determine appropriate equations and parameters for the various functions. The procedure for choosing the best-fit equations was the same for all the functions modeled in this paper. Equations were fit to data using the Levenberg-Marquardt algorithm (Press *et al.*, 1986; Brown *et al.*, 1996b), a least-squares non-linear curve-fitting technique. The convergence criteria set for this iterative algorithm was a 0.01% improvement in the numerical error of fit. Unless specifically stated, data from all relevant experiments were combined when fitting an equation. For functions that had been modeled previously, equations were taken or adapted from the literature. For novel functions, we developed and tested many equations but present here only the results of those that could fit the data well with minimal complexity and coefficients.

Results

Morphometric data collected from these animals, including sarcomere length measurements, anatomical range of motion, muscle weight, muscle length and peak tetanic force, were included as part of a larger study on CF morphometry and published previously in Brown *et al.* (1998b). The values for these measurements for all animals used in this study were typical of those reported and hence are not repeated here.

Force-length relationships

Isometric passive FL relationships (for PE1) were collected in every animal. These data were used after the experiment to remove the passive component of total recorded force, leaving the active component as was required for subsequent analysis. Passive force data were collected in the isometric state 30 ms after stretching to at least 15 different lengths. Forces were normalized to F_0 (maximal potentiated isometric force) and lengths were normalized to L_0 (fascicle length at which F_0 was recorded). Data from three animals are plotted in Figure 2 to demonstrate the complete range of passive forces observed in these experiments. Passive FL relationships from different animals did not tend to normalize well with respect to each other as noted previously (Brown *et al.*, 1996a). Thus, each data set was fit independently to equation 4 with best-fit curves for the associated data sets plotted in Figure 2 (best-fit constants listed in Table 1).

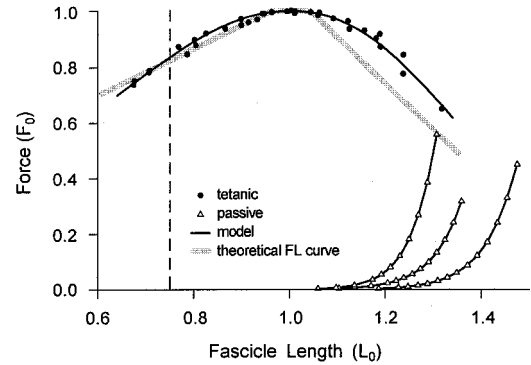


Fig. 2. Active isometric tetanic FL data and passive (F_{PE1}) FL data. All tetanic data to the left of the dashed line at $0.75 L_0$ were plotted after subtracting F_{PE2} from the total force (as described in text). Data are indicated with circles (tetanic) or triangles (passive) while the best-fit curves are drawn with a thin black line (equations 4 and 6). The theoretical tetanic FL curve based upon filament overlap (Herzog *et al.*, 1992) is shown with the thick gray line.

$$F_{PE1}(L) = c_1 k_1 \ln \left\{ \exp \left[\frac{(L - L_{r1})}{k_1} \right] + 1 \right\} \quad (4)$$

(from Brown *et al.*, 1996b)

As suggested previously by Brown *et al.* (1996b), we needed to include a second passive force (F_{PE2}) that resisted compression at lengths shorter than $0.75 L_0$. Because we collected only a few data points at short lengths (insufficient to estimate accurately F_{PE2} for CF), we assumed for the purposes of estimating F_{PE2} that feline CF was identical to feline soleus (SOL). Equation 5 was then used to model this passive force with the best-fit constants (listed in Table 1) taken directly from Brown *et al.* (1996b).

$$F_{PE2}(L) = c_2 \{ \exp[k_2(L - L_{r2})] - 1 \}, \quad F_{PE2} \leq 0 \quad (5)$$

(from Brown *et al.*, 1996b)

Potentiated isometric tetanic FL data (collected at the end of a 10 p train at 120 pps) were collected from five animals, in contrast to dispotentiated FL data which were collected in all experiments (see Materials and methods). Maximal potentiated isometric tetanic force was less than the maximal dispotentiated isometric force ($92 \pm 2\%$, mean \pm SD; $n = 5$), presumably due to some form of short-term fatigue as described previously (Brown and Loeb, 1998b). This scaling factor was used to estimate F_0 for those experiments in which only dispotentiated isometric tetanic data were collected. Both F_{PE1} and F_{PE2} were subtracted from total force to determine active force. The combined data from five experiments are plotted in Figure 2 along with the theoretical FL relationship based upon filament overlap (Herzog *et al.*, 1992). The active force measurements are reasonably similar to the theoretical relationship, although they are somewhat larger for lengths longer than L_0 . Using equation 6, a best-fit curve was determined for the combined FL data and plotted in Figure 2 (best-fit constants listed in Table 1).

$$FL(L) = \exp\left(-\text{abs}\left|\frac{L^B - 1}{\omega}\right|^p\right)$$

(from Otten, 1987; Brown *et al.*, 1996b) (6)

Isometric FL relationships at sub-tetanic stimulus frequencies were collected from five animals. Complete data sets (5 stimulus frequencies ranging from 15–120 pps at each of six lengths ranging from ca. 0.65 to 1.25 L_0) were collected in two experiments whereas partial data sets (15 data points over similar ranges) were collected in the other three experiments. Sample force traces from one experiment are shown in Figure 3. At 1.0 L_0 CF produced progressively greater forces as stimulus frequency increased from 15 to 120 pps (Figure 3A). At a stimulus frequency of 30 pps CF produced progressively greater forces as length was increased from ca. 0.8 to 1.2 L_0 (Figure 3B). The complete interactive effects of length and stimulus frequency are seen more clearly in Figure 3C, in which the complete FL relationships at 15, 30, 40, 60 and 120 pps are plotted for one experiment (all sub-tetanic data points were collected 133 ms after stimulus onset). The isometric FL relationships at different stimulus frequencies are not congruent. To remove the effects of filament overlap so that the residual effects of length upon activation could be seen more clearly, the data in Figure 3C were normalized to the tetanic data (Figure 3D). At all sub-tetanic stimulus frequencies, activation increased as length was increased. This effect was proportionally stronger at lower stimulus frequencies.

The interactive effects of stimulus frequency and length were examined from a different perspective by plotting activation-frequency (Af) relationships at different lengths. Af relationships for three of the lengths in Figure 3D (ca. 0.8, 1.0, 1.2 L_0) are plotted in Figure 4A along with similar data from a second experiment. When viewed in this format the interactive effects of stimulus frequency and length appear simpler; increases in length shift the Af relationship to lower stimulus frequencies. While this shifting effect is consistent from one animal to the next, the basic Af relationship does not scale well between animals. To solve this problem we normalized all stimulus frequencies to $f_{0.5}$, the stimulus frequency required to produce 0.5 F_0 at 1.0 L_0 . When the data from the two experiments in Figure 4A are normalized in this manner, the two data-sets become congruent (Figure 4B). The mean $f_{0.5}$ (\pm SD) recorded in these experiments was 34 ± 4 pps ($n = 6$).

Numerous novel equations were fit to the Af data; only equation 7, which produced the best overall fit, is listed here (best-fit constants for equation 7 are listed in Table 1). To ensure accuracy over the whole range of stimulus frequencies, the errors used by the curve-fitting algorithm were weighted by 1/activation. A sample of the fit is shown in Figure 4C along with the partial data-set from one animal. The relationship between this Af sub-element and the other sub-elements in the final model is shown schematically in Figure 11. Although there are three constants listed in equation 7, Af was forced to be equal to 0.5 when $f = 1$ and $L = 1$, resulting in a relationship between a_f and n_{f0} not listed here.

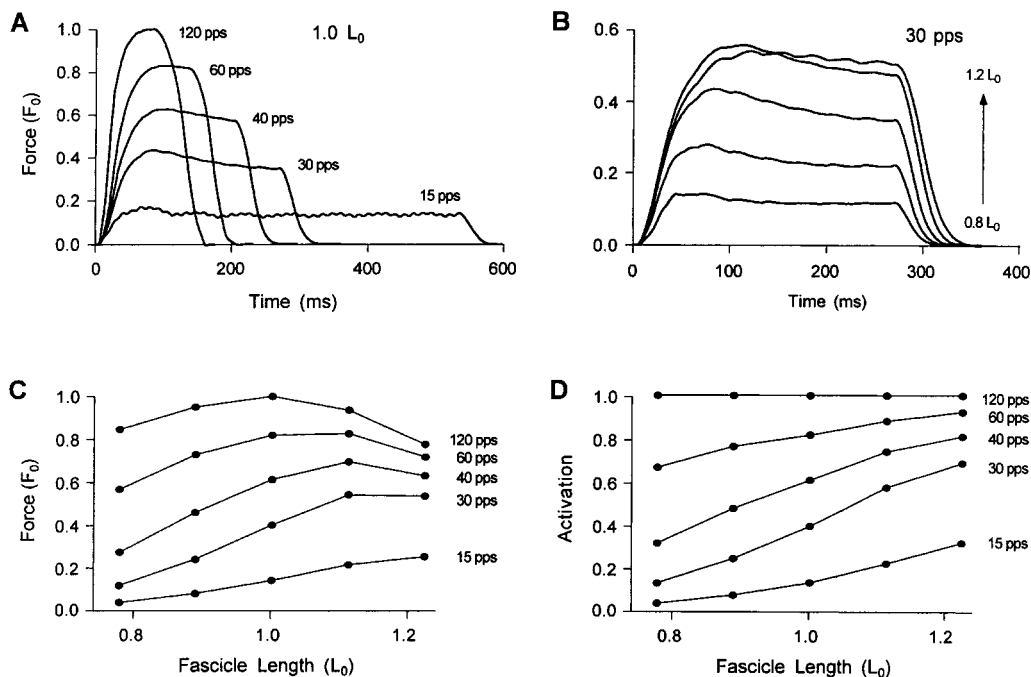


Fig. 3. Sub-tetanic FL relationships. Sample force traces from one experiment are shown in A and B to illustrate the effect of changing stimulus frequency (A) or fascicle length (B) on isometric force. The complete FL data set for one experiment is shown in C, with data points collected 133 ms after stimulus onset (100 ms after stimulus onset for 120 pps data). The FL relationships at different stimulus frequencies are not congruent. The effects of filament overlap were removed in this data set by normalizing the forces to the tetanic data (shown in D), which revealed strong length dependencies of activation that were independent of filament overlap.

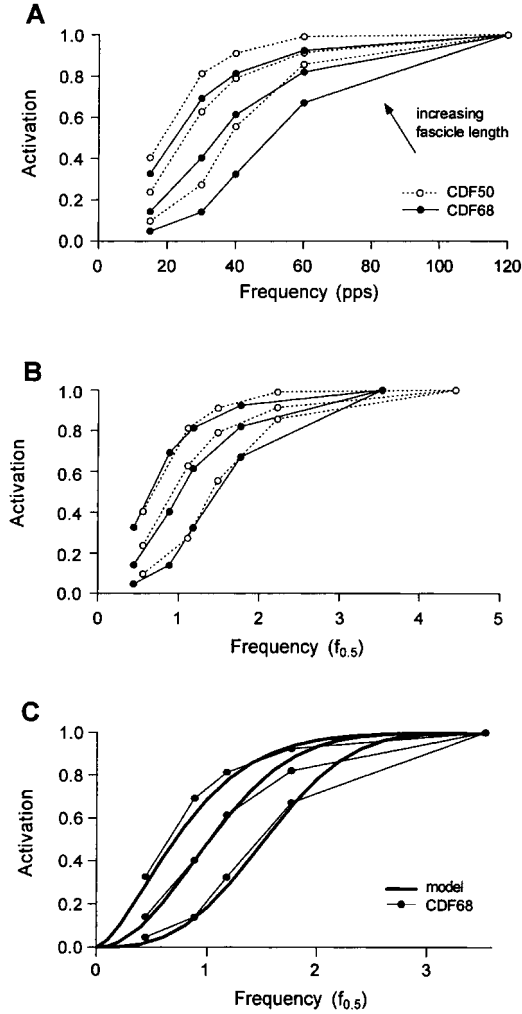


Fig. 4. Activation-frequency relationships. A. The Af relationships at three different lengths ranging from ca. 0.8 to 1.2 L_0 are shown for each of two experiments. Increases in length shifted the Af relationship to lower frequencies. Although the shifting effect is similar for the two data sets, the two data sets are not congruent. To normalize the data, we scaled all stimulus frequencies by $f_{0.5}$, the stimulus frequency required to produce 0.5 F_0 at 1.0 L_0 . The data in A were replotted in B to demonstrate the effect of this normalization (values of $f_{0.5}$ were 27 and 34 pps for the two data sets). C. One data set from B is replotted here along with the best-fit curves produced by equation 7.

$$Af(f, L) = 1 - \exp \left[- \left(\frac{f}{a_f n_f} \right)^{n_f} \right],$$

$$n_f = n_{f0} + n_{f1} \left(\frac{1}{L} - 1 \right) \quad (7)$$

As mentioned previously, F_{PE2} is a passive force resisting compression at short muscle lengths. It was introduced originally by Brown *et al.* (1996b) to account for apparent length dependencies in the shortening half of the FV relationship for lengths shorter than 0.75 L_0 . (These dependencies disappeared when F_{PE2} was introduced.) Originally, however, PE2 was assumed to be completely passive (i.e. $F_{PE} = F_{PE1} + F_{PE2}$). The predictions of our model using FL, Af and an *activation-independent* version of F_{PE2} are shown for one data

set in Figure 5A (model 'A'), including data points at lengths less than 0.75 L_0 . This version produces a discrepancy at short lengths (see arrow in Figure 5A and scatter plot of errors in Figure 5B). If we assume that F_{PE2} scales with recruitment and activation (as indicated previously in equation 3 and discussed in the Appendix) the model fits more accurately (model 'B' in Figure 5C and D).

Force-velocity relationships

Tetanic FV relationships for potentiated CF at 0.8 and 1.1 L_0 have been published previously and included a strong length dependence for shortening velocities and no length dependence for lengthening velocities (Brown and Loeb, 1999b). Because Brown and Loeb's data were limited to velocities no greater than 1.0 L_0/s for active stretches, further experiments were conducted in four animals to extend the tetanic FV relationship out to 3.5 L_0/s . To avoid damage from active lengthening (Brown and Loeb, 1995) we limited the active stretches to lengths less than 0.9 L_0 . As described above, passive forces were subtracted from the data and the effects of filament overlap removed by normalizing to isometric force. The mean (\pm SD) data from Brown and Loeb (1999b) combined with those from the current study are plotted in Figure 6. Equation 8 was adapted from Brown *et al.* (1996b) to include a length dependence for shortening velocities and no length dependence for lengthening velocities. The shortening half of this equation is mathematically equivalent to the classical Hill equation (Hill, 1938) when the length dependence is removed. The best-fit curves are plotted in Figure 6 (best-fit constants listed in Table 1).

$$FV(V, L) = \begin{cases} \frac{V_{\max} - V}{V_{\max} + (c_{V0} + c_{V1}L)V}, & V \leq 0 \\ \frac{b_V - a_V V}{b_V + V}, & V > 0 \end{cases} \quad (8)$$

(adapted from Brown *et al.*, 1996b)

Complete FV relationships for sub-tetanic stimulus frequencies were collected from three animals. Data sets included five velocities ($-3.0, -0.5, 0.0, 0.5$ and $2.0 L_0/s$) at each of five length-frequency pairs (20 pps at 0.95 L_0 , 40 pps at each of 0.8, 0.95 and 1.1 L_0 and 60 pps at 0.95 L_0). Further sub-tetanic FV data at other length-frequency pairs (including 20 and 60 pps at 1.1 L_0) were collected from one of those animals as well as from a fourth animal. For two of the complete data sets, shortening or stretching began 35 ms prior to data collection, whereas for all other data it began at 45 ms prior. There was no obvious difference between the results produced by the different protocols. Sample force traces from one experiment are shown in Figure 7A and 7B to illustrate the complex effects of length and stimulus frequency on force. Summary FV relationships were

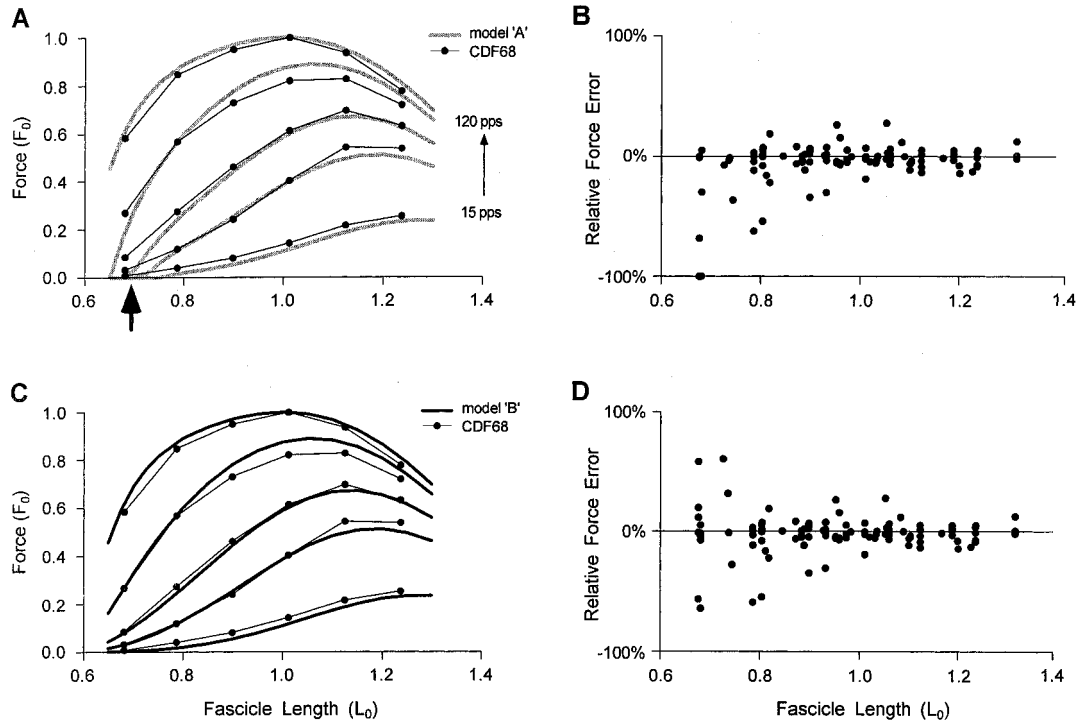


Fig. 5. The effects of F_{PE2} . A, C. Isometric FL data originally plotted in Figure 3C is replotted here including additional data from short lengths ($<0.75 L_0$). Two best-fit models are plotted with these data for comparison. In model 'A', F_{PE2} is independent of activation (as originally proposed by Brown *et al.*, 1996b) whereas in model 'B', F_{PE2} scales with activation (as proposed here in equation 3 and in the Appendix). Parts B and D show the relative force errors of the two models respectively where relative error is defined as $(\text{model_prediction} - \text{force_data}) / \text{force_data}$. The model is more accurate at short lengths when F_{PE2} scales with activation.

constructed by collecting data points 150 ms after stimulus onset (templates were pre-designed so that trials at various velocities all passed through the same length at $t = 150$ ms). Mean (\pm SD) data from three experiments are plotted in Figure 7C and D to compare the effects of stimulus frequency (at $0.95 L_0$) or the effects of length (at 40 pps) on the FV relationship. All forces were normalized to the isometric force at the corresponding length and stimulus frequency to remove filament overlap effects and apparent differences in

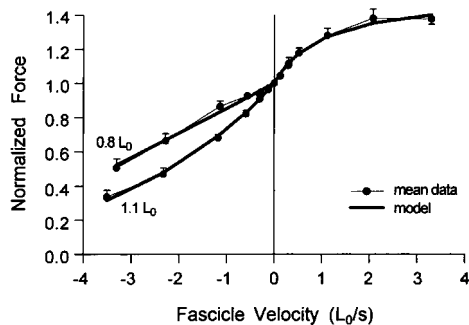


Fig. 6. Tetanic FV relationships. Mean tetanic FV data ($n = 3$ or 4 for all data points; \pm SD) are plotted separately for two different lengths (0.8 and $1.1 L_0$) for shortening velocities and combined for several short lengths (0.8 – $0.95 L_0$) for lengthening velocities. Lengthening velocities were defined as positive. Forces were normalized to isometric force. Data for shortening velocities were published previously by Brown and Loeb (1999b). Data from that study was combined with new data from this study for lengthening velocities. The best-fit curve using equation 8 is plotted as a thick line.

activation. Lower stimulus frequencies and shorter lengths both had the apparent effect of decreasing the slope of the FV relationship, in some cases even making the curve non-monotonic (e.g. $0.8 L_0$ data at 40 pps in Figure 7D).

In order to determine if the effects of length and stimulus frequency on the FV relationship observed in Figure 7 reflected changes in the instantaneous FV relationship, we examined more closely the effects of shortening and stretching on the force transients. Force traces at various lengths and stimulus frequencies were normalized to the force produced just prior to either shortening or stretching and compared to each other. To remove the effects of sag (a short-term drop in force within a single contraction unique to fast-twitch muscle; Burke *et al.*, 1973), we divided the force trace at each point in time by the corresponding force trace from a complementary isometric trial at the same stimulus frequency and length. Sample force traces normalized in this manner are plotted in Figure 8 for shortening at $-3.0 L_0/s$ and for stretching at $2.0 L_0/s$. As can be seen in Figure 8A and B, there was no effect of stimulus frequency on the normalized force transients during the first 20 ms for either shortening or stretching (shaded region). These observations were confirmed statistically by correlating normalized force 20 ms after the start of a length change with stimulus frequency ($n = 3$ at each of 20, 40 and 60 pps and $n = 1$ at 120 pps; $r = 0.51, 0.27$ for shortening and lengthening respectively, $P > 0.1$ for both). Similarly, there was no effect of

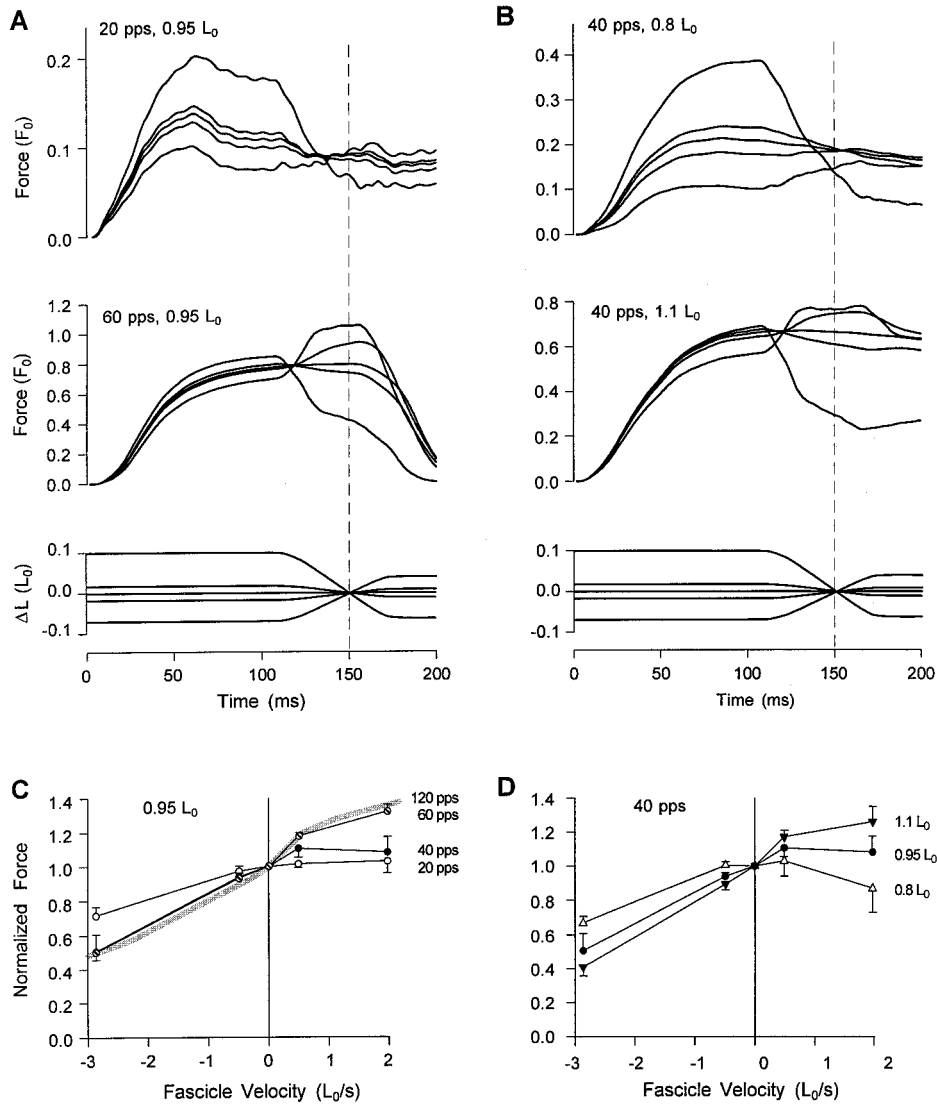


Fig. 7. Sub-tetanic FV relationships. **A, B.** Sample force traces demonstrating the effects of either frequency (**A**) or length (**B**) on force. Stretching an active muscle always increased force relative to its pre-stretch force, however, that force was not always greater than the force produced by a complementary isometric trial at the same length (compare forces at dashed line). Conversely, shortening always reduced force compared to pre-shortening, and that force was not always less than the force produced by a complementary isometric trial at the same length. These effects are clearer in the summary FV relationships plotted in **C** and **D**. Mean data (\pm SD) for all sub-tetanic data are from three experiments. Data are normalized to isometric force. Tetanic data (120 pps, thick gray line) for shortening velocities at 0.95 L_0 were estimated by taking the mean of the data collected at 0.8 and 1.1 L_0 (as plotted in Figure 6). Reducing stimulus frequency or length both appeared to ‘flatten’ the FV relationships.

length on the normalized force transients during active stretches (Figure 8D; $n = 3$ at each of three lengths; $r = 0.38$, $P > 0.1$). In contrast, there was a residual effect of length on the force transients during the first 20 ms of shortening: less force was produced at longer lengths (Figure 8C; $r = 0.93$, $P < 0.001$). These length-related findings are consistent with the length dependence of the tetanic FV relationship described previously (Brown and Loeb, 1999b) and shown here in Figure 6.

To model the effects described above we replaced the length input to the Af relationship with a time-delayed version of length. We called this new length input the ‘effective’ length (L_{eff}), as shown in equation 9. The effect of introducing this time delay was to cause a muscle to

‘remember’ the activation level associated with its previous lengths (see Discussion). The relationship between this sub-element and the other sub-elements in the final model is shown schematically in Figure 11. Equation 10 was found to produce the best-fit time delay from a number of possibilities (best-fit constants listed in Table 1). Equation 10 was fit to the normalized FV data to ensure an accurate fit at all levels of activation. (Because of the cube in the numerator, the ‘time constant’ for equation 10 should be thought of as $T_L * (1 - Af)/(L - L_{\text{eff}})^2$; for $L - L_{\text{eff}} = 0.03$ and $Af = 0.5$, the time constant is ca. 50 ms.) The best-fit sub-tetanic FV relationships predicted by equations 8, 9, and 10 are shown in Figure 9 along with the mean data plotted previously in Figure 7.

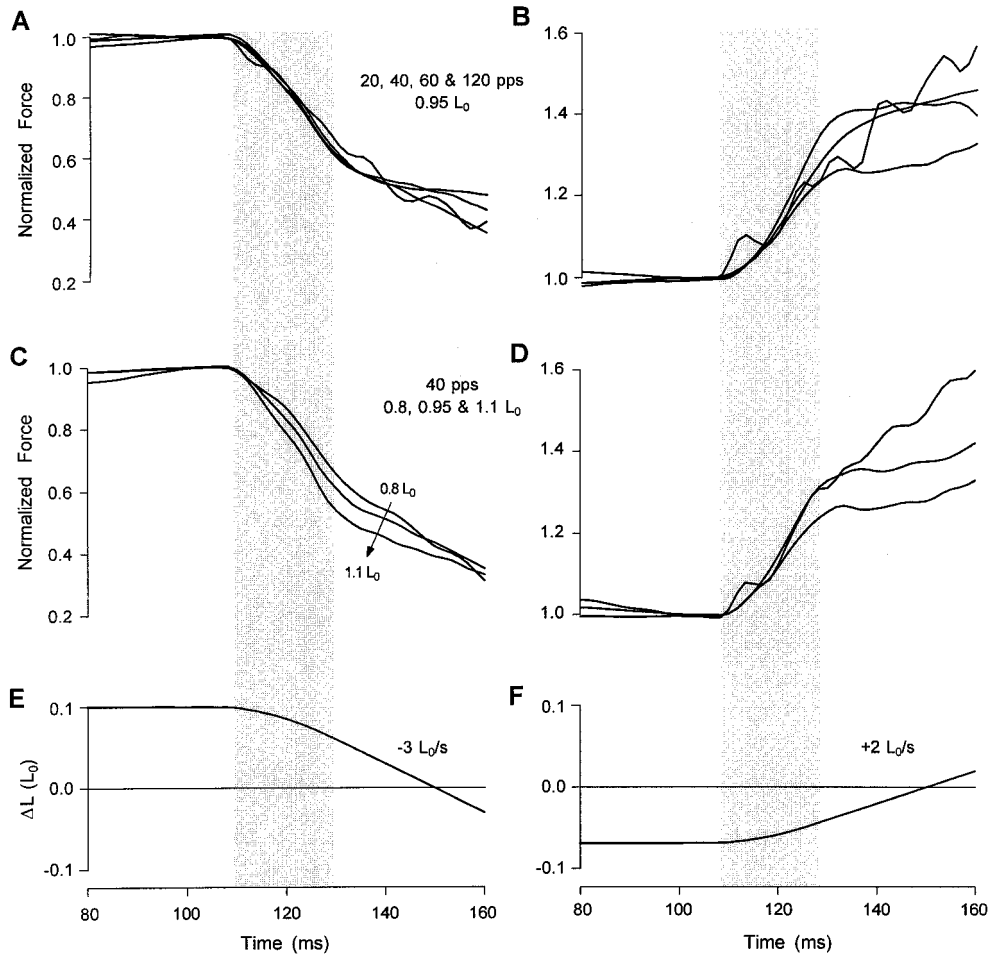


Fig. 8. ‘Instantaneous’ effects of shortening or lengthening. **A, B.** Sample force traces demonstrating the effects of stimulus frequency on force during the initial portion of a length change, normalized for the effects of static length, frequency and ‘sag’ as described in the text. Stimulus frequency had no effect on the normalized force transients during the first 20 ms for either shortening or stretching (shaded region). **C, D.** Sample force traces demonstrating the effects of length on force during the initial portion of a length change. Forces were normalized and analyzed as described in **A** and **B**. There was no effect of length on normalized force during the first 20 ms of active stretches whereas there was a residual effect of length during shortening: less relative force was produced at longer lengths. **E, F.** Fascicle length transients corresponding to the force traces in **A–D**.

$$Af(f, L_{\text{eff}}) = 1 - \exp\left[-\left(\frac{f}{a_f n_f}\right)^{n_f}\right],$$

$$n_f = n_{f0} + n_{f1}\left(\frac{1}{L_{\text{eff}}} - 1\right)$$

(new form of equation 7) (9)

$$\dot{L}_{\text{eff}}(t) = \frac{[L(t) - L_{\text{eff}}(t)]^3}{T_L(1 - Af)} \quad (10)$$

Slow-twitch muscle

Our slow-twitch model was based partly upon the work of Brown *et al.* (1996b) who previously published best-fit constants for FL, FV, F_{PE1} and F_{PE2} for feline SOL. Because the equation used by Brown *et al.* for the FV relationship had a different form than the one presented here, we combined our equation 8 with equations 10, 12 and 16 from Brown *et al.* (1996b) to produce a generic

equation (equation 11; best-fit constants for both slow- and fast-twitch muscle are listed in Table 1). We assumed initially for our slow-twitch model that the Af relationship (normalized to $f_{0.5}$) and T_L (time constant determining L_{eff}) were identical for slow- and fast-twitch muscle.

$$FV(V, L) = \begin{cases} \frac{V_{\text{max}} - V}{V_{\text{max}} + (c_{V0} + c_{V1}L)V}, & V \leq 0 \\ \frac{b_V - (a_{V0} + a_{V1}L + a_{V2}L^2)V}{b_V + V}, & V > 0 \end{cases} \quad (11)$$

(new form of equation 8)

To test the accuracy of our slow-twitch model, we compared its predictions to data collected previously from feline SOL using experimental methods similar to those described here. Because the whole-muscle SOL preparation includes a large series elastic element, we added one to our model using the equations and parameters suggested by Brown *et al.* (1996b; F_{SE} equation has the same form as equation 4 for F_{PE1} ;

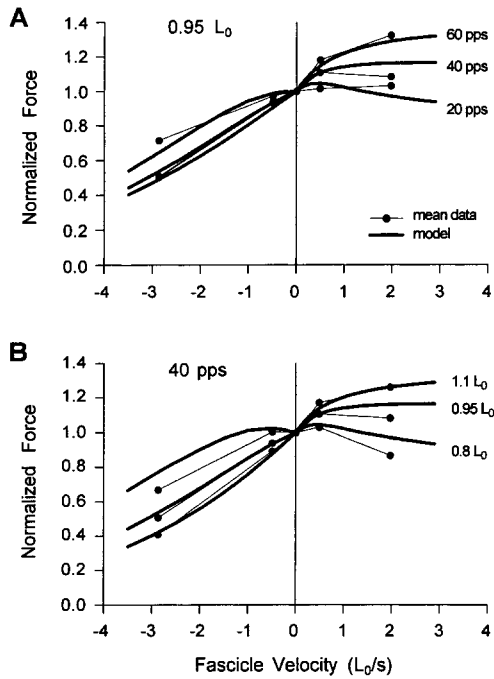


Fig. 9. Model of sub-tetanic FV relationships. **A, B.** The mean sub-tetanic data from three experiments (plotted originally in Figure 7C and **D**) are plotted against the best-fit curves from the model (equations 8, 9 and 10).

best-fit constant listed in Table 1). We chose an appropriate ratio of SE length to fascicle length for SOL (1.9) based upon the anatomical measurements of Scott *et al.* (1996).

Our isometric FL predictions were compared with the data plotted in Figure 8 of Rack and Westbury (1969). An appropriate L_0 (5.0 cm) was estimated by fitting our model to their tetanic data at 35 pps. Because Rack and Westbury incorrectly used whole-muscle lengths to determine passive force, we included this error in our model predictions. The error arises because fascicle length during an isometric whole-muscle contraction is shorter than fascicle length during rest. Fascicle length determines passive force and so passive forces actually change during a whole-muscle isometric contraction (see Scott *et al.*, 1996 for more detail). We then estimated $f_{0.5}$ (5.5 pps) from the sub-tetanic data plotted in their Figure 8. The model predictions are plotted here along with Rack and Westbury's data in Figure 10A. Using the Af relationship for CF, the model predicts the qualitative relationships accurately, but does not do a good job of predicting the quantitative relationships (dashed lines in Figure 10A). Inspection of the results suggested that SOL has a greater length dependence for Af as compared to CF. By manually changing one of the parameters for the Af relationship, we were able to produce a much better fit (solid line, Figure 10; manually chosen 'best-fit' constants listed in Table 1).

In order to test the ability of our slow-twitch model to predict FV relationships we compared its predictions against isovelocicity data published previously by Joyce *et al.* (1969). For this simulation L_0 was estimated as

3.0 cm to fit their tetanic FV data (35 pps). For sub-tetanic stimulus frequencies, our model over-estimated relative force considerably for both lengthening and shortening velocities (dashed lines, Figure 10B). This was not surprising given that our model did not yet account for yielding. To incorporate yielding into our model we assumed that Joyce *et al.* (1969) were correct that the rate of cross-bridge detachment increases during lengthening (and also during shortening), thus reducing the steady-state number of attached cross-bridges. We introduced a scaling factor Y to account for yielding and used it to scale the normalized stimulus frequency in the Af relationship (re-introduced as equation 12). The relationship between this yielding sub-element and the other sub-elements in the final model is shown schematically in Figure 11 in the Discussion. We chose to scale frequency rather than activation so that our model could account for the differential effect of yielding observed at different stimulus frequencies; yielding is greatest at moderate levels of activation corresponding to the steepest portion of the Af relationship (Joyce *et al.*, 1969) and non-existent at tetanic stimulus frequencies. Y was defined to be equal to 1 during the isometric condition and to be less than 1 during length changes.

$$Af(f, L_{\text{eff}}, Y) = 1 - \exp\left[-\left(\frac{Yf}{a_f n_f}\right)^{n_f}\right],$$

$$n_f = n_{f0} + n_{f1}\left(\frac{1}{L_{\text{eff}}} - 1\right)$$

(new form of equation 9) (12)

The form of Y must account for two other important factors. Yielding is not instantaneous; its effect on force develops over hundreds of ms (e.g. Figures 2, 3 and 6 of Joyce *et al.*, 1969). The amount of yielding is velocity-dependent; there is less yielding at low velocities compared to higher velocities (Figure 5 of Joyce *et al.*, 1969). We introduced equation 13 to account for these various effects. The parameter V_Y , which controls the velocity sensitivity of the amount of yielding, was estimated from the shape of the 7 pps FV relationship from Figure 5 of Joyce *et al.* (1969), which are replotted here in Figure 10B. The parameters T_Y and c_Y , which control the time constant and maximum amount of yielding respectively, were then estimated manually by trial and error by comparing our simulation results with the data from Figures 3 and 5 of Joyce *et al.* (1969), Figure 5 of Nichols and Houk (1976) and Figure 7 of Cordo and Rymer (1982). Sample force traces from our model under various conditions are shown in Figure 10C; they show effects similar to those reports (original data not shown). The isovelocicity FV relationships predicted by this yielding model are shown as solid lines in Figure 10B and demonstrate that inclusion of a yielding term resulted in a much better fit.

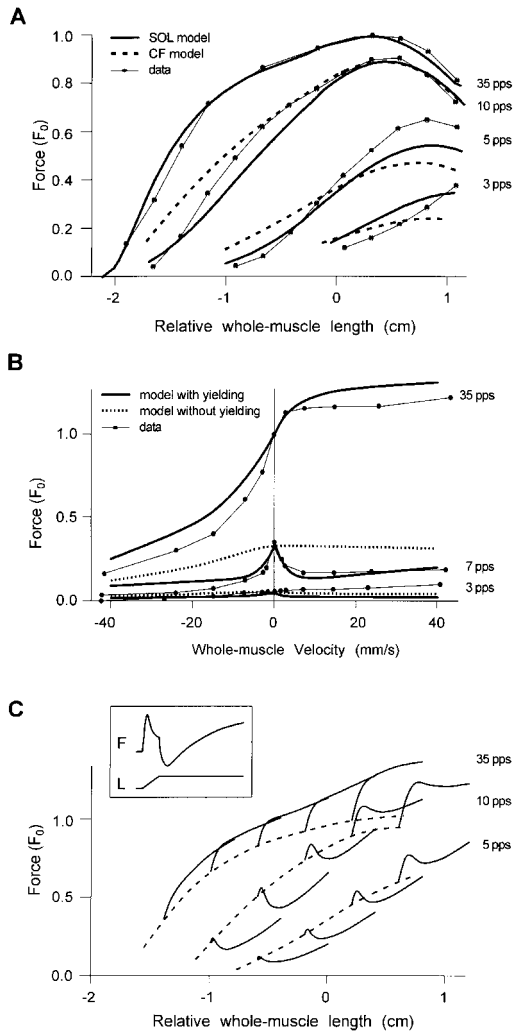


Fig. 10. Slow-twitch model. **A.** Isometric FL data from feline SOL collected by Rack and Westbury (1969, Fig. 8) are replotted here with best-fit versions of two models: our fast-twitch model (dashed line) based on CF but with stimulus frequency scaled by SOL's $f_{0.5}$ and our slow-twitch model (solid lines); both models are identical for tetanic activation (35 pps for SOL). Whole-muscle length (fascicle plus aponeurosis plus tendon) is given relative to optimal muscle length as per Rack and Westbury (1969). **B.** Isovelocity data from feline SOL collected by Joyce *et al.* (1969, Fig. 5) are replotted here with best-fit versions of two models: our slow-twitch models without yielding (dotted line) and with yielding (solid line); both models are identical for tetanic 35 pps stimuli. All movements began 5 mm from a length approximately equal to an ankle angle of 70° (Joyce *et al.*, 1969). **C.** Sample force transients produce by slow-twitch yielding model. The main plot is organized in the same fashion as in Joyce *et al.*, (1969, Fig. 3). Whole-muscle length (fascicle plus aponeurosis plus tendon) is given relative to optimal muscle length as per Joyce *et al.* (1969). The muscle was 'stimulated' isometrically until it reached a steady-state force after which it was stretched at 7.2 mm/s for 6 mm. Only the force transients during stretch are plotted as a function of length. Dashed lines indicate the isometric FL relationship. The inset traces show a single force transient and associated length transient (to be compared to data plotted in Nichols and Houk (1976, Fig. 5), transients are exactly 1 s long). The muscle was stimulated at 8 pps isometrically until steady-state force was reached, followed by a 2 mm stretch at 12.5 mm/s. Only the transients just before, during and after the stretch are shown.

$$\dot{Y}(t) = \frac{1 - c_Y [1 - \exp(-\text{abs}|V|/V_Y)] - Y(t)}{T_Y} \quad (13)$$

Discussion

The data and model presented here provide an accurate description of the force produced by potentiated fast-twitch muscle operating over physiological fascicle lengths, velocities and stimulus frequencies. While the effects of length and stimulus frequency have been well studied before, we provide new evidence here of the interactions among length, velocity and stimulus frequency. In particular we showed that the strong effects of both length and stimulus frequency on sub-tetanic FV relationships are not mediated through changes in the instantaneous FV relationship. Instead the effects appear to be mediated through a time delay in the length dependence of the activation-frequency relationship.

Interactions between stimulus frequency and isometric length

The qualitative effects of length and stimulus frequency on isometric force in CF were as expected based upon previous reports. Passive FL relationships (PE1) were quasi-exponential and did not scale well between animals, as reported for other feline hindlimb muscles (Brown *et al.*, 1996a). In contrast, the active tetanic FL relationship did scale well between animals and its shape resembled closely the shape of the theoretical FL relationship based upon filament overlap (Herzog *et al.*, 1992). At sub-tetanic stimulus frequencies the peak of the isometric FL shifted to lengths greater than L_0 , as found previously in feline SOL (Rack and Westbury, 1969) and mouse flexor brevis (Balnave and Allen, 1996). As a measure of the relative force-length-frequency characteristics of potentiated CF, we determined the stimulus frequency necessary to produce $0.5 F_0$ at $1.0 L_0$ ($f_{0.5}$). The mean $f_{0.5}$ for potentiated CF was 34 ± 4 pps, which compares reasonably well with the fast-twitch data available for other feline muscles after taking into account the effects of dispotentiation (which increases the measured $f_{0.5}$) and length (the activation-frequency relationship shifts to lower frequencies at longer lengths). These estimates are 59 ± 13 pps for dispotentiated flexor carpi radialis motor units (Botterman *et al.*, 1986), $>39 \pm 8$ pps for dispotentiated peroneus longus motor units (experiments conducted at $L > L_0$; Kernell *et al.*, 1983) and >25 – 30 pps for dispotentiated flexor digitorum longus motor units (experiments conducted at $L > L_0$; Powers and Binder, 1991). In comparison, values of $f_{0.5}$ reported for feline slow-twitch muscle include 5–6 pps for soleus whole muscle (Rack and Westbury, 1969), 23 ± 6 pps for flexor carpi radialis motor units (Botterman *et al.*, 1986) and $>18 \pm 4$ pps for peroneus longus motor units (experiments conducted at $L > L_0$; Kernell *et al.*, 1983).

The effects of length on the Af relationship described here are analogous to the effects of length on

the force-pCa relationships measured from skinned fiber preparations (Moiescu and Thieleczek, 1979; Stephenson and Williams, 1982; Moss *et al.*, 1983); increases in length shift both relationships to lower concentrations of Ca^{2+} (assuming that lower stimulus frequencies are associated with lower concentrations of Ca^{2+} ; Balnave and Allen, 1996). These effects have been postulated to be mediated by length-dependent changes in the rate of cross-bridge attachment and detachment (Yang *et al.*, 1998; Brown and Loeb, 1999b). Alternatively, the length-dependencies of Af could be explained by changes in steady-state intracellular Ca^{2+} . It has been shown recently that the site of Ca^{2+} release (the triads) is located halfway along the thin filament in CF, independent of sarcomere length (Brown *et al.*, 1998a). The diffusion distances from the site of Ca^{2+} release to Ca^{2+} binding and uptake are thus length-dependent, providing at least one hypothetical mechanism for a Ca^{2+} -related length dependence. This effect would have to be temperature- (or species)-dependent, however, because Balnave and Allen (1996) observed no effect of length on steady-state intracellular Ca^{2+} in mouse flexor brevis fibers at 22°C.

When testing our model's ability to predict correctly the isometric FL data at short lengths, we discovered that an activation-independent F_{PE2} did not work well. A simple analysis of the behavior of the thick filament under compression (presented in the Appendix) revealed that F_{PE2} should, in fact, depend upon activation. Using the simple assumption that the thick filament buckles in a bistable manner under compression, we showed that F_{PE2} should be linearly proportional to activation as well as linearly proportional to the amount of compression. Both of these predictions agree well with our model.

Interactions between stimulus frequency and length and velocity

The effects of both length and stimulus frequency on the sub-tetanic FV properties of whole muscle have never been examined systematically before and were remarkably strong in CF. Joyce *et al.* (1969) did look at the effect of stimulus frequency on sub-tetanic FV properties at one length in feline SOL, but their results were affected by the phenomenon of yielding, which does not occur in CF. The normalized force transients presented in Figure 8 suggested to us that length had little effect and stimulus frequency had no effect on the 'instantaneous' FV properties of CF. The effects of stimulus frequency and length on the sub-tetanic FV relationships in Figure 7 could not, therefore, be explained through changes in the instantaneous FV relationship; instead we believe that there may be a time delay between a change in length and the associated change in the length-dependent Af relationship. Consider the effects of active lengthening at 2.0 L_0/s at 0.8 L_0 (40 pps; Figure 7B). In comparison to the corre-

sponding isometric contraction, the active stretch produced less force at $t = 150$ ms. Recruitment and filament overlap are identical at this instant in time while the tetanic FV relationship predicts that the active stretch should produce more force than the isometric. By process of elimination (using equation 2 – $F_{\text{CE}} = R \cdot \text{Af} \cdot \text{FL} \cdot \text{FV}$) we can conclude that there must be a lower level of activation (i.e. Af) during the active stretch. How could this be? The active stretch began at a shorter fascicle length which we know corresponds to less activation (Figure 3D). If we assume that length dependent changes in Af occur with a time delay, then as a muscle is stretched, it will 'remember' its lower level of activation from its shorter initial length and it will produce less force than expected. For the converse situation in which a muscle is shortening, it would 'remember' the higher activation that it had at its longer initial lengths and so it would produce greater force than expected. At shorter lengths and lower stimulus frequencies where activation has a greater relative length dependence (Figure 3D) one would then expect a greater effect on the FV relationship; this was observed in our experiments (Figure 7C and D).

We have suggested above two possible mechanisms for the Af length dependence: changes in the rate of cross-bridge attachment/detachment and/or changes in steady-state levels of intracellular Ca^{2+} . If either of these mechanisms really occurs, then there would necessarily be a time delay associated with their effects. Furthermore, if there is cooperativity between cross-bridges (as suggested by Moss, 1992; Swartz and Moss, 1992; Metzger, 1995), then any change in the number of cycling cross-bridges would feed back onto itself through a change in cooperativity, leading to a further change in the number of cycling cross-bridges and so on, adding an additional time delay.

Our hypothesis of a time delay in the Af length-dependence is consistent with several other observations. The effects of length on the instantaneous FV relationship (as estimated from the normalized force transients of Figure 8) were identical to the effects of length on the tetanic FV relationship (Figure 6). At tetanic stimulus frequencies, activation is maximal so changes in length will not affect Af; any effects of length on the tetanic FV relationship should thus reflect changes in the instantaneous FV relationship, consistent with our findings. In work using maximally activated, skinned single fiber preparations (in which intracellular Ca^{2+} is controlled), Ford *et al.* (1991) have shown that decreasing lattice spacing via osmotic compression results in lower relative forces at moderate speeds of shortening. This finding is analogous to the effect of decreasing lattice spacing via increasing muscle length in tetanically stimulated whole muscle, which also results in lower relative forces at moderate speeds of shortening. Furthermore, Ford *et al.* showed in an osmotically compressed fiber that changes in activation via changes in intracellular Ca^{2+} had no effect on the relative FV relationship for shortening velocities. These results are

consistent with our findings using a whole-muscle preparation in which activation was controlled by stimulus frequency.

Yielding

Yet another effect that is dependent upon a muscle's recent kinematic history is that of yielding. In contrast to feline SOL, which exhibits a strong yielding effect (Rack and Westbury, 1969; Nichols and Houk, 1976), feline CF does not yield. These findings are consistent with single fiber work by Malamud *et al.* (1996), who demonstrated that slow-twitch fibers from a number of feline muscles exhibit strong yielding behavior whereas fast-twitch fibers from the very same muscles did not yield until very high velocities of stretch were imposed (e.g. 2–10 L_0/s). Malamud *et al.* further observed a correlation between short-range stiffness (stiffness exerted over length changes less than 0.5% L_0) and yielding, suggesting that these two phenomena might share a common mechanism. We agree with Rack and Westbury's original hypothesis that a greater rate of cross-bridge detachment during active lengthening as compared to the isometric condition could reduce the number of force-producing cross-bridges during stretch. If this increase in cross-bridge detachment occurred suddenly (i.e. at a critical sarco-

mere extension) then this would lead to the observed yielding behavior. To explain fiber type differences, we propose that the increase in cross-bridge detachment rate that occurs suddenly during stretch at the critical sarcomere extension is masked in fast-twitch muscle by the greater rate of cross-bridge attachment in fast-twitch muscle. Thus, yielding would only be seen in fast-twitch muscle at higher velocities when the detachment rate becomes fast enough such that high rates of attachment can no longer mask it.

The model

This model represents a substantial improvement over most previous models of muscle because it extends its predictive power to include the complex effects of stimulus frequency on the FL and FV relationships for the sub-tetanic frequencies at which motor units normally operate (Bigland and Lippold, 1954; Bellemare *et al.*, 1983; Hoffer *et al.*, 1987). Furthermore, it accounts for the different behaviors of slow- and fast-twitch muscle, including the yielding behavior unique to slow-twitch muscle. The model's form and the relationships between its various sub-elements are shown schematically in Figure 11. The model's equations and best-fit constants for both fast- and slow-twitch muscle

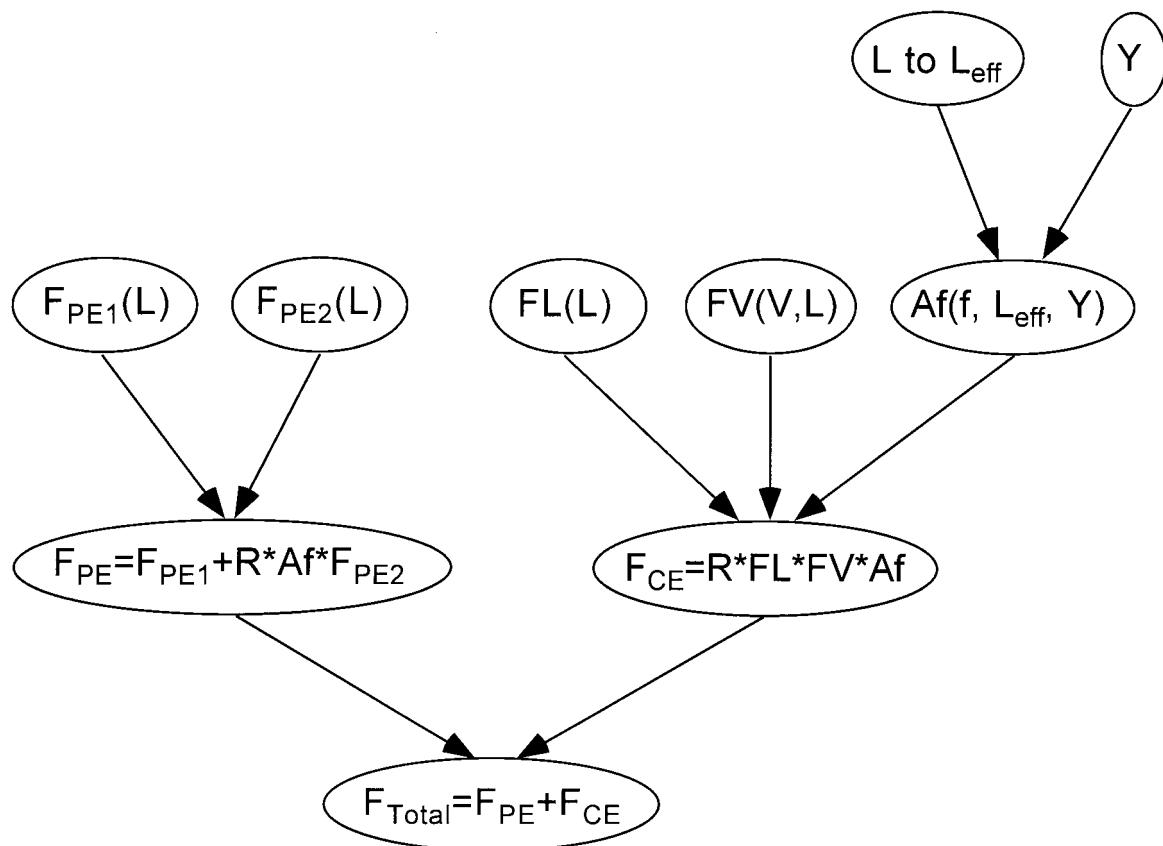


Fig. 11. Schematic description of muscle model sub-elements. The equations associated with each sub-element are listed in Table 1. F_{total} , total force produced by muscle fascicles; F_{PE} , total passive force produced by parallel elastic element PE (see Figure 1); F_{CE} , total active force produced by contractile element CE (see Figure 1); F_{PE1} , passive elastic force produced when stretched; F_{PE2} , passive elastic force resisting compression produced when fascicles are short; R, recruitment; FL, tetanic force-length relationship; FV, tetanic force-velocity relationship; Af, Activation-frequency relationship; Y, yielding factor; L, fascicle length; L_{eff} , effective fascicle length; V, fascicle velocity; f stimulus frequency.

Table 1. Summary of model equations and best-fit constants. The basic form of the model is summarized in equations 1–3 and is not repeated here. The relationships between the various sub-elements are shown schematically in Figure 11. The best-fit constants for F_{PE1} , F_{PE2} , FL and FV for slow-twitch muscle as well as F_{SE} were based upon feline SOL and were taken or adapted from Brown *et al.* (1996b). The best-fit constants for Af, L_{eff} and Y for slow-twitch muscle were based upon data published previously by Rack and Westbury (1969), Joyce *et al.* (1969) and Nichols and Houk (1976). All fast-twitch parameters were based upon the results of this study using feline CF. F_{PE1} does not scale well between animals so three examples each for both fast- and slow-twitch muscle are given. For F_{SE} , L^T is defined as the length of the SE (tendon plus aponeurosis) in units of L_0^T (the length of the SE when stretched by 1.0 F_0 ; Brown *et al.*, 1996b). Although there are three constants listed for each of F_{SE} , F_{PE1} and Af, only two are independent due to constraints (e.g. Af = 0.5 when $f_{eff} = 1$ and $L_{eff} = 1$)

Curve	Constants for fast-twitch muscle				Constants for slow-twitch muscle			
$F_{SE}(L^T) = c^T k^T \ln \left\{ \exp \left[\frac{(L^T - L_r^T)}{k^T} \right] + 1 \right\}$	c^T	k^T	L_r^T		c^T	k^T	L_r^T	
	(same as slow-twitch)				27.8	0.0047	0.964	
$F_{PE1}(L) = c_1 k_1 \ln \left\{ \exp \left[\frac{(L - L_{r1})}{k_1} \right] + 1 \right\}$		c_1	k_1	L_{r1}		c_1	k_1	L_{r1}
	CDF59	25.6	0.059	1.54	SOL10	355	0.040	1.35
	CDF73	31.8	0.046	1.34	SOL11	76.4	0.053	1.40
	CDF77	69.6	0.058	1.50	SOL12	67.1	0.056	1.41
$F_{PE2}(L) = c_2 \{ \exp[k_2(L - L_{r2})] - 1 \}$, $F_{PE2} \leq 0$	c_2	k_2	L_{r2}		c_2	k_2	L_{r2}	
	(same as slow-twitch)				-0.020	-18.7	0.79	
$FL(L) = \exp \left(-\text{abs} \left[\frac{L^B - 1}{\omega} \right]^{\rho} \right)$	ω	β	ρ		ω	β	ρ	
	0.81	1.55	2.12		1.26	2.30	1.62	
$FV(V, L) = \begin{cases} \frac{V_{\max} - V}{V_{\max} + (c_{v0} + c_{v1}L)V}, & V \leq 0 \\ \frac{b_V - (a_{v0} + a_{v1}L + a_{v2}L^2)V}{b_V + V}, & V > 0 \end{cases}$	V_{\max}	c_{v0}	c_{v1}		V_{\max}	c_{v0}	c_{v1}	
	-7.39	-3.21	4.17		-4.06	5.88	0	
	a_{v0}	a_{v1}	a_{v2}	b_V	a_{v0}	a_{v1}	a_{v2}	b_V
	-1.53	0	0	1.05	-4.70	8.41	-5.34	0.18
$Af(f, L_{eff}, Y) = 1 - \exp \left[- \left(\frac{Yf}{a_f n_f} \right)^{n_f} \right]$, $n_f = n_{f0} + n_{f1} \left(\frac{1}{L_{eff}} - 1 \right)$	a_f	n_{f0}	n_{f1}		a_f	n_{f0}	n_{f1}	
	0.56	2.11	3.31		0.56	2.11	5	
$\dot{L}_{eff}(t, L, Af) = \frac{[L(t) - L_{eff}(t)]^3}{T_L(1 - Af)}$	T_L (ms)				T_L (ms)			
	0.088				(same as fast-twitch)			
$\dot{Y}(t, V) = \frac{1 - c_Y [1 - \exp(-\text{abs}[V]/V_Y)] - Y(t)}{T_Y}$	c_Y	V_Y	T_Y (ms)		c_Y	V_Y	T_Y (ms)	
	0	-	-		0.35	0.1	200	

(based upon feline CF and SOL respectively) are summarized in Table 1. By introducing the stimulus-frequency scaling parameter $f_{0.5}$, we have made the model more generic in its ability to describe the force-producing properties of different muscles and fiber types. The main kinematic effect that we have not incorporated is that of stretch-induced force enhancement and shortening-induced force depression resulting from changes in fascicle velocity; this effect will be described and discussed in a subsequent paper (in preparation).

The model presented here is based on a strategy of decomposing the emergent behaviors of muscle into constituent components having a one-to-one correspondence with anatomical components and physiological processes (Brown and Loeb, 1999a). For example, by understanding the nature of the mechanism(s) responsible for the effects of length and stimulus frequency on the sub-tetanic FV relationships, we were able to account for them with a relatively simple addition to our model and be reasonably confident that it would work for conditions that we had not yet tested. This approach can be contrasted to the more fundamental approach of Zahalak's distributed moment (DM) approximation (Zahalak, 1981). The DM model makes assumptions about the distribution of states occupied by

cycling cross-bridges and calculates force based upon this distribution. The effects of various kinematics on force simply emerge as inherent properties of the system as the distribution of states changes with changes in kinematics. For example, with appropriate parameters the DM model can replicate yielding behavior of slow-twitch muscle (Zahalak, 1986). The ability of the DM model to 'naturally' account for many of the intrinsic properties of muscle makes it genuinely attractive. Its main disadvantage, and the reason we chose not to use it, is that the DM model is inherently more complex than the one presented here.

The next step that needs to be undertaken to expand our model is to incorporate the effects of dynamic changes in activation. This will include the effects of rise and fall times on force as well as the effects of sag (as occurs in fast-twitch muscle). Rise and fall time data have been presented so far only for twitch and tetanic conditions (Brown and Loeb, 1999b). These effects interact with length and stimulus frequency (Brown and Loeb, unpublished observations) and so will require significant work to be incorporated into our model. Once completed, we will have a mathematical model of muscle that accounts well for almost all of the important effects on force output that are known to occur in mammalian skeletal muscle under physiologically relevant conditions.

Acknowledgements

The authors would like to thank Janet Creasy, David Kim and Kim Moore for technical assistance with the experiments, and Dr Frances J.R. Richmond for comments on our manuscript. This research was funded by the Medical Research Council of Canada.

Appendix

Demonstration that PE2 is activation-dependent

The following analysis demonstrates one way in which the passive force-resisting compression (F_{PE2}) could conceivably depend upon activation. It assumes that any changes in thick filament length occur through some sort of buckling (i.e. non-elastic compression). We assume that the thick filament is bistable in compression: for stresses less than F_{crit} , the thick filament length does not change from its uncompressed length; for regions of the thick filament in which compression stresses are greater than F_{crit} , that region of the thick filament crumples a fixed fraction of its length (δ). For simplicity, we also assume that thick filament compression does not alter the relative force-producing ability of cross-bridges within the compressed region (see below). As shown in Figure A1, let us consider a half-sarcomere. Let x represent the distance along the thick filament from the z-band. Let $F_{x\text{-bridges}}(x)$ represent the total force of all cross-bridges in the thick filament region up to x as determined by equation A1.

$$F_{x\text{-bridges}}(d) = A_r f_x n_x d \quad (\text{A1})$$

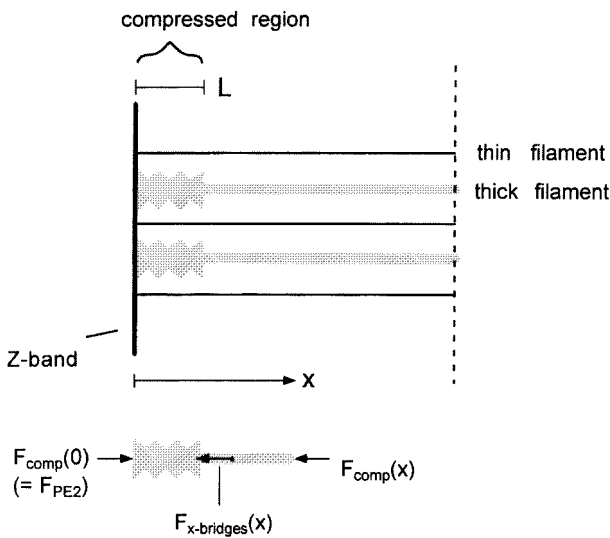


Fig. A1. Half-sarcomere schematic for a length sufficiently short to cause thick filament compression. Let x represent the distance from the Z-band along the thick filament. At some distance $x = L$, the thick filament changes from compressed to uncompressed state. $F_{x\text{-bridges}}(x)$ is defined as the total force of all cross-bridges in the thick filament region up to x . $F_{comp}(x)$ is defined as the compressive force experienced in the thick filament at point x . $F_{comp}(0)$ equals F_{PE2} .

where: A_r represents the relative activation level (between 0 and 1), f_x the force/cross-bridge and n_x the density of cross-bridges per unit length.

Let us further define the compressive force experienced in the thick filament at point x as $F_{comp}(x)$, as shown in Figure A1. $F_{comp}(0)$ thus represents the force exerted on the thick filament by the Z-band (which is equal to F_{PE2}). When the thick filament is compressed, there will be some distance $x = L$ which identifies the separation point between the compressed region of the thick filament and the uncompressed region; at this point, $F_{comp}(L) = F_{crit}$. Therefore $F_{comp}(x)$ is greater than F_{crit} for x less than L (i.e. in the compressed region). Thus the forces of all the cross-bridges up to $x = L$ equals the compressive force from the Z-band minus F_{crit} as summarized in equation A2.

$$F_{x\text{-bridges}}(L) = F_{comp}(0) - F_{comp}(L) = F_{comp}(0) - F_{crit} \quad (\text{A2})$$

Recalling that the compressed region of the thick filament is compressed by the fraction δ , we can calculate the amount of compression that the thick filament is experiencing (x_{comp}).

$$x_{comp} = \delta L \quad (\text{A3})$$

Re-arranging to solve for L and plugging back into equations A1 and A2 to solve for $F_{comp}(0)$ produces:

$$\begin{aligned} F_{comp}(0) &= F_{x\text{-bridges}}(L) + F_{crit} \\ &= A_r f_x n_x L + F_{crit} \\ &= A_r f_x n_x x_{comp} / \delta + F_{crit} \end{aligned} \quad (\text{A4})$$

According to this simple analysis, F_{PE2} [i.e. $F_{comp}(0)$] is approximately proportional to A_r (if F_{crit} is negligible then F_{PE2} is exactly proportional to A_r). Furthermore, F_{PE2} increases in a linear fashion with x_{comp} , which resembles closely our proposed form of F_{PE2} (see Figures 2 and 6 of Brown *et al.*, 1996b). F_{PE2} also depends upon f_x (force/cross-bridge), which under normal conditions will depend upon velocity through the FV function. In the thick filament region that has buckled through compression, however, there will be no relative motion between the cross-bridges and the thin filament even when sarcomere velocity is not zero, so f_x in the buckled region will be independent of sarcomere velocity (i.e. F_{PE2} will be independent of FV). If one of our assumptions was incorrect and cross-bridge formation in the buckled zone tends to be impaired or ineffectual, then A_r will have little effect on F_{PE2} (the first term in equation A4 will disappear, and F_{comp} will be equal to F_{crit}). If we instead had assumed that the thick filament compressed elastically with no buckling, then a similar analysis (not shown here) would produce a relationship in which F_{PE2} is dependent on $A_r^{0.5}$. Thus the dependence upon activation is specific to some, but not all of the above assumptions. Given that our results are

best modeled with $F_{\text{comp}}(0) = A_{r,x} n_x x_{\text{comp}} / \delta$, (remembering that $F_{\text{comp}}(0) = F_{\text{PE2}}$) we can tentatively suggest that F_{crit} is small enough as to be negligible in mammalian skeletal muscle and that thick filament compression is approximated well by simple buckling. This hypothesis, however, will need to be verified with experimental paradigms designed specifically for this purpose.

References

- Ariano MA, Armstrong RB and Edgerton VR (1973) Hindlimb muscle fiber populations of five mammals. *J Histochem Cytochem* **21**: 51–55.
- Balnavae CD and Allen DG (1996) The effect of muscle length on intracellular calcium and force in single fibres from mouse skeletal muscle. *J Physiol* **492**: 705–713.
- Bellemare F, Woods JJ, Johansson R and Bigland-Ritchie BR (1983) Motor-unit discharge rates in maximal voluntary contractions of three human muscles. *J Neurophysiol* **50**: 1380–1392.
- Bigland B and Lippold OCJ (1954) Motor unit activity in the voluntary contraction of human muscle. *J Physiol* **125**: 322–335.
- Botterman BR, Iwamoto GA and Gonyea WJ (1986) Gradation of isometric tension by different activation rates in motor units of cat flexor carpi radialis muscle. *J Neurophysiol* **56**: 494–506.
- Brown IE, Liinamaa TL and Loeb GE (1996a) Relationships between range of motion, L_0 and passive force in five strap-like muscles of the feline hindlimb. *J Morphol* **230**: 69–77.
- Brown IE, Scott SH and Loeb GE (1996b) Mechanics of feline soleus: II. Design and validation of a mathematical model. *J Muscle Res Cell Motil* **17**: 219–232.
- Brown IE, Kim DH and Loeb GE (1998a) The effect of sarcomere length on triad location in intact feline caudofemoralis muscle fibers. *J Muscle Res Cell Motil* **19**: 473–477.
- Brown IE, Satoda T, Richmond FJR and Loeb GE (1998b) Feline caudofemoralis muscle. Muscle fiber properties, architecture, and motor innervation. *Exp Brain Res* **121**: 76–91.
- Brown IE and Loeb GE (1995) A damaged state in cat caudofemoralis muscle induced by high forces. *Can J Physiol Pharmacol* **73**: Ai(Abtract).
- Brown IE and Loeb GE (1998a) A physiological model of the dynamic force-producing properties of mammalian fast-twitch skeletal muscle. *Soc Neurosci Abstr* **24**: 1672 (Abstract).
- Brown IE and Loeb GE (1998b) Post-activation potentiation: a clue for simplifying models of muscle dynamics. *Am Zool* **38**: 743–754.
- Brown IE and Loeb GE (1999a) A reductionist approach to creating and using neuromusculoskeletal models. In: Winters JM and Crago PE (eds) *Biomechanics and Neural Control of Movement* Springer-Verlag, New York.
- Brown IE and Loeb GE (1999b) Measured and modeled properties of mammalian skeletal muscle. I. The effects of post-activation potentiation on the time-course and velocity dependencies of force production.
- Burke RE, Levine DN, Tsairis P and Zajac FE (1973) Physiological types and histochemical profiles in motor units of the cat gastrocnemius. *J Physiol* **234**: 723–748.
- Chizeck HJ (1992) Adaptive and nonlinear control methods for neuroprostheses. In: Stein RB, Peckham HP and Popovic D (eds) *Neural Prostheses: Replacing Motor Function after Disease or Disability* (pp. 298–328). Oxford University Press, New York.
- Close RI (1972) The relations between sarcomere length and characteristics of isometric twitch contractions of frog sartorius muscle. *J Physiol* **220**: 745–762.
- Cooper S and Eccles JC (1930) The isometric responses of mammalian muscles. *J Physiol* **69**: 377–385.
- Cordo PJ and Rymer WZ (1982) Contributions of motor-unit recruitment and rate modulation of compensation for muscle yielding. *J Neurophysiol* **47**: 797–809.
- Durfee WK and Palmer KI (1994) Estimation of force-activation, force-length, and force-velocity properties in isolated, electrically stimulated muscle. *IEEE Trans Biomed Engng* **41**: 205–216.
- Ford LE, Nakagawa K, Desper J and Seow CY (1991) Effect of osmotic compression on the force-velocity properties of glycerinated rabbit skeletal muscle cells. *J Gen Physiol* **97**: 73–88.
- Gribble PL and Ostry DJ (1996) Origins of the power law relation between movement velocity and curvature: modeling the effects of muscle mechanics and limb dynamics. *J Neurophysiol* **76**: 2853–2860.
- Hatze H (1977) A myocybernetic control model of skeletal muscle. *Biol Cybernet* **25**: 103–119.
- Herzog W, Kamal S and Clarke HD (1992) Myofilament lengths of cat skeletal muscle: theoretical considerations and functional implications. *J Biomech* **25**: 945–948.
- Hill AV (1938) The heat of shortening and the dynamic constants of muscle. *Proc R Soc Lond (Biol)* **126**: 136–195.
- Hoffer JA, Sugano N, Loeb GE, Marks WB, O'Donovan MJ and Pratt CA (1987) Cat hindlimb motoneurons during locomotion: II. Normal activity patterns. *J Neurophysiol* **57**: 530–553.
- Joyce GS, Rack PMH and Westbury DR (1969) Mechanical properties of cat soleus muscle during controlled lengthening and shortening movements. *J Physiol* **204**: 461–474.
- Kernell D, Eerbeek O and Verhey BA (1983) Relation between isometric force and stimulus rate in cat's hindlimb motor units of different twitch contraction times. *Exp Brain Res* **50**: 220–227.
- Krylow AM and Rymer WZ (1997) Role of intrinsic muscle properties in producing smooth movements. *IEEE Trans BME* **44**: 165–176.
- Loeb GE, Brown IE and Cheng EJ (1999) A hierarchical foundation for models of sensorimotor control. *Exp Brain Res* **126**: 1–18.
- Malamud JG, Godt RE and Nichols TR (1996) Relationship between short-range stiffness and yielding in type-identified, chemically skinned muscle fibers from the cat triceps surae muscles. *J Neurophysiol* **76**: 2280–2289.
- Metzger JM (1995) Myosin binding-induced cooperative activation of the thin filament in cardiac myocytes and skeletal muscle fibers. *Biophys J* **68**: 1430–1442.
- Moiescu DG and Thieleczek R (1979) Sarcomere length effects on the Sr^{2+} - and Ca^{2+} -activation curves in skinned frog muscle fibres. *Biochim Biophys Acta* **546**: 64–76.
- Moss RL, Swinford A and Greaser ML (1983) Alterations in the Ca^{2+} sensitivity of tension development by single skeletal muscle fibers at stretched lengths. *Biophys J* **43**: 115–119.
- Moss RL (1992) Ca^{2+} regulation of mechanical properties of striated muscle. Mechanistic studies using extraction and replacement of regulatory proteins. [Review]. *Circ Res* **70**: 865–884.
- Nichols TR and Houk JC (1976) Improvement in linearity and regulation of stiffness that results from actions of stretch reflex. *J Neurophysiol* **39**: 119–142.
- Otten E (1987) A myocybernetic model of the jaw system of the rat. *J Neurosci Meth* **21**: 287–302.
- Powers RK and Binder MD (1991) Effects of low-frequency stimulation on the tension-frequency relations of fast-twitch motor units in the cat. *J Neurophysiol* **66**: 905–918.
- Press WH, Flannery BP, Teukolsky SA and Vetterling WT (1986) *Numerical Recipes*. Cambridge University Press, Cambridge, UK.
- Rack PMH and Westbury DR (1969) The effects of length and stimulus rate on tension in the isometric cat soleus muscle. *J Physiol* **204**: 443–460.
- Roszek B, Baan GC and Huijing PA (1994) Decreasing stimulation frequency-dependent length-force characteristics of rat muscle. *J Appl Physiol* **77**: 2115–2124.
- Scott SH, Brown IE and Loeb GE (1996) Mechanics of feline soleus. I. Effect of fascicle length and velocity on force output. *J Muscle Res Cell Motil* **17**: 205–218.
- Scott SH and Loeb GE (1995) The mechanical properties of the aponeurosis and tendon of the cat soleus muscle during whole-muscle isometric contractions. *J Morphol* **224**: 73–86.
- Stephenson DG and Wendt IR (1984) Length dependence of changes in sarcoplasmic calcium concentration and myofibrillar calcium

- sensitivity in striated muscle fibres. *J Muscle Res Cell Motil* **5**: 243–272.
- Stephenson DG and Williams DA (1982) Effects of sarcomere length on the force-pCa relation in fast-and slow-twitch skinned muscle fibres from the rat. *J Physiol* **333**: 637–653.
- Swartz DR and Moss RL (1992) Influence of a strong-binding myosin analogue on calcium-sensitive mechanical properties of skinned skeletal muscle fibers. *J Biol Chem* **267**: 20497–20506.
- Westerbald H, Duty S and Allen DG (1993) Intracellular calcium concentration during low-frequency fatigue in isolated single fibers of mouse skeletal muscle. *J Appl Physiol* **75**: 382–388.
- Westerbald H and Allen DG (1991) Changes of myoplasmic calcium concentration during fatigue in single mouse muscle fibers. *J Gen Physiol* **98**: 615–635.
- Yang Z, Stull JT, Levine RJC and Sweeney HL (1998) Changes in interfilament spacing mimic the effects of myosin regulatory light chain phosphorylation in rabbit psoas fibers. *J Struct Biol* **122**: 139–148.
- Zahalak GI (1981) A distribution-moment approximation for kinetic theories of muscular contraction. *Math Biosci* **55**: 89–114.
- Zahalak GI (1986) A comparison of the mechanical behavior of the cat soleus muscle with a distribution-moment model. *J Biomech Eng* **108**: 131–140.
- Zajac FE (1989) Muscle and tendon: Properties, models, scaling and application to biomechanics and motor control. *Crit Rev Biomed Engng* **17**: 359–411.